Single-molecule diffusion reveals similar mobility for the Lck, H-ras, and K-ras membrane anchors

Lommerse, P.; Vastenhoud, K.; Pirinen, N.J.; Magee, A.I.; Spaink, H.P.; Schmidt, T.

Single-Molecule Diffusion Reveals Similar Mobility for the Lck, H-Ras, and K-Ras Membrane Anchors

Piet H. M. Lommerse,*† Karin Vastenhoud,*† Niina J. Pirinen,‡ Anthony I. Magee,‡ Herman P. Spaink,† and Thomas Schmidt*

*Physics of Life Processes, Leiden Institute of Physics, and †Department of Molecular Cell Biology, Institute of Biology, Leiden University, Leiden, The Netherlands; and ‡Division of Biomedical Sciences, Imperial College London, London, United Kingdom

ABSTRACT Recent evidence on the occurrence of small (5–700 nm diameter) lipid microdomains in the exoplasmic leaflet of the plasma membrane has evoked interest in the possibility that similar domains may also be present in the cytoplasmic leaflet of the plasma membrane. However, current knowledge about these "lipid rafts", in live cells is limited. One way to obtain insight into the occurrence and the size of lipid rafts is the use of single-molecule microscopy, which allows one to study the diffusive motion of individual molecules with high positional and temporal accuracy. Using this technique, we compared the diffusion behavior of the Lck membrane anchor, which has a high affinity for lipid rafts, to the diffusion behavior of the K-Ras membrane anchor, which has negligible affinity for rafts and compared the results with those of the H-Ras membrane anchor. Surprisingly, we found only minor differences in the diffusion behavior of the various lipid anchors, indicating that putative cytoplasmic leaflet lipid rafts would have to be small (<137 nm diameter) and do not affect the mobility of membrane-anchored molecules much on timescales up to 60 ms.

INTRODUCTION

The plasma membrane of mammalian cells is heterogeneous in structure and contains several types of domains (1). One of the causes of small membrane domains (300–600 nm) is a network of membrane-associated actin, which can cause temporal trapping of lipids and membrane proteins (2). Another type of membrane domains are lipid microdomains (3), also called ''lipid rafts''. These are structures in which saturated acyl chain lipids and cholesterol pack together resulting in a liquid-ordered phase that sets these lipid areas apart from the liquid-disordered bulk plasma membrane (4). Lipid rafts contain a variety of proteins, whose association with these domains is typically biochemically tested by measuring their partitioning into the detergent-resistant membrane (DRM) fraction (5). It was speculated that association of particular sets of proteins with lipid rafts plays an important role in a variety of signal transduction pathways (6).

Most experiments to directly measure and visualize lipid rafts have been performed by labeling molecules localized in the exoplasmic leaflet. Raft sizes measured vary from ~5 to 700 nm (7–12). Much less is known, however, about the existence, size, and nature of lipid raft like domains in the cytoplasmic leaflet. Model membrane experiments indicated that mixtures of phospholipids resembling those found in the cytoplasmic leaflet do not spontaneously form liquid-ordered domains (13). However, a recent study (14) suggested that cholesterol-dependent clusters could be present in the cytoplasmic leaflet of live cells.

A possible link between lipid rafts in the exoplasmic and cytoplasmic leaflet is potentially of great importance as the transduction of cellular signals from the outside to the inside of the cell usually involves proteins anchored in the cytoplasmic leaflet of the plasma membrane. Well-known examples are small GTPases and Src-family kinases, which have different membrane anchors. The small GTPase K-Ras has a C-terminal membrane anchoring sequence that consists of a farnesyl moiety in conjunction with a polybasic domain. This type of anchor has a negligible affinity for lipid rafts and hence the K-Ras anchor is generally used as a nonraft marker (15). In contrast, the Src-kinase Lck is anchored via two cysteine-linked S-acyl groups and one glycine-linked myristoyl group at the N-terminus of the protein. The Lck anchor confers a high affinity for lipid rafts (16–19) . By comparing the diffusion of the K-Ras anchor and the Lck anchor at short time and small length scales we intended to obtain more information on the presence and dimensions of putative lipid rafts in the cytoplasmic leaflet. To be able to directly follow the motion of the membrane anchors we fused them to the enhanced yellow-fluorescent protein (eYFP) and studied their diffusion at the single-molecule level in live cells. The high positional accuracy of the technique (~35 nm) enabled us to detect even small membrane domains (>137 nm diameter). Diffusion analysis of thousands of single-molecule trajectories of both the Lck and K-Ras membrane anchor revealed an unexpected similarity. Both anchors showed a major, fast-diffusing fraction and a minor, slow-diffusing fraction. The fast-diffusing fraction of the Lck-anchor and the K-Ras anchor contained 84% and 73% of the molecules, respectively. For both anchors, this fast

Submitted December 2, 2005, and accepted for publication April 28, 2006.

Address reprint requests to T. Schmidt, Physics of Life Processes, Leiden Institute of Physics, Leiden University, Niels Bohrweg 2, 2333 CA Leiden, The Netherlands. Tel.: 31-71-527-5982; Fax.: 31-71-527-5819; E-mail: schmidt@physics.leidenuniv.nl.

0006-3495/06/08/1090/08 $2.00

doi: 10.1529/biophysj.105.079053

fraction showed free diffusion with diffusion coefficients of 1.3 $\mu m^2/s$ for the Lck anchor and 1.0 $\mu m^2/s$ for the K-Ras anchor. The remaining fraction of molecules of both anchors was confined in ~200 nm sized domains. As these domains contained a considerable fraction of both anchors, they are most likely not lipid rafts. The lack of clear differences between these two membrane anchors supports models of the cytoplasmic leaflet in which proposed lipid rafts are small (<137 nm diameter, the detection limit of our technique) and do not affect the mobility of molecules much on timescales at least up to 60 ms.

MATERIALS AND METHODS

DNA constructs

A double-stranded synthetic oligonucleotide encoding the human Lck membrane anchoring sequence (amino-acids MGCGCSSHPED) with 5′ *Hind*III and 3′*Bam*HI restriction sites was cloned into the pcDNA3 vector (Invitrogen, Paisley, UK). This vector contained the entire coding sequence of eYFP, which was previously cloned into the *Bam*HI and *Xho*I sites. A linker region (amino acids VDPPVAT) was incorporated between the Lck and eYFP sequences. The eYFP K-Ras membrane anchor construct was a gift from J. Hancock (20).

Cell cultures

In this study a mouse fibroblast cell line (3T3-A14) was used and cultured in DMEM medium supplemented with streptomycin (100 μg/ml), penicillin (100 U/ml), and 10% bovine serum in a 7% CO_2 humidified atmosphere at 37°C (95% humidity). Cells were used for 12–14 passages and were transferred every 4 days. For microscopy the cells were cultured on No. 1 glass slides (Fisher Scientific, 's-Hertogenbosch, The Netherlands). Cells exhibiting a confluency level of 20–30% were used for transfection with 1.0 μg DNA and 3 μl FuGENE 6 (Roche Molecular Biochemicals, Indianapolis, IN) per glass slide. The transfection efficiency, as determined by fluorescence microscopy, was ~30%.

Observation and tracking of single-molecules

The experimental arrangement for single-molecule imaging has been described in detail previously (21–23). Briefly, cells adherent to glass slides were mounted onto the microscope and kept in phosphate-buffered saline (PBS: 150 mM NaCl, 10 mM Na_2HPO_4/NaH_2PO_4, pH 7.4) at 37°C. For the observation of the mobility of the membrane-anchored fluorophores the focus was set to the apical membrane of the cells (depth of focus ~1 μm). The density of fluorescent proteins on the plasma membrane of selected transfected cells (5–6 days posttransfection) was $<1\ \mu m^{-2}$, which permitted imaging and tracking of individual fluorophores and ensured that fluorescent protein dimerization (14) was minimized.

Fluorescence images were taken consecutively with up to 1000 images per sequence. By connectivity analysis between consecutive images the two-dimensional trajectories of individual molecules in the plane of focus were reconstructed (21). These trajectories were up to 9 steps in length, mainly limited by the blinking and photobleaching of the fluorophore (22). To compensate for the limited length of individual trajectories, multiple data sets, each consisting of hundreds of trajectories from 8–21 cells per construct, were analyzed. Moreover, for each cell, several separate data sets were acquired, each with a different time between consecutive images (time lag, t_{lag}). By using different time lags, varying from 5 to 60 ms, the diffusion behavior of the membrane-anchored molecules was studied.

Models to analyze square displacement distributions

The trajectories were analyzed following a method developed earlier (24). In brief, the lateral diffusion of Brownian particles in a medium characterized by a diffusion constant D is described by the cumulative probability distribution function for the square displacements, r^2 (25,26):

$$P(r^2, t_{lag}) = 1 - \exp\left(-\frac{r^2}{r_0^2(t_{lag})}\right). \quad (1)$$

$P(r^2, t_{lag})$ describes the probability that the Brownian particle starting at the origin will be found within a circle of radius r at time t_{lag}. It is characterized by the mean-square displacement of $r_0^2(t_{lag}) = 4Dt_{lag}$ (25) and gives a good description of lipid diffusion in a free-standing membrane (27). Provided that the system under study segregates into two components, one with a fast and one with a slow mobility, characterized by mean-square displacements r_1^2 and r_2^2, and relative fractions α and $(1 - \alpha)$, respectively, Eq. 1 becomes (24):

$$P(r^2, t_{lag}) = 1 - \left[\alpha \times \exp\left(-\frac{r^2}{r_1^2(t_{lag})}\right) + (1-\alpha)\cdot \exp\left(-\frac{r^2}{r_2^2(t_{lag})}\right)\right]. \quad (2)$$

The cumulative probability distributions $P(r^2, t_{lag})$ were constructed for each time lag from the single-molecule trajectories, obtained from 8–21 different cells, by counting the number of square displacements with values $\leq r^2$, and subsequent normalization by the total number of data points (24). Probability distributions with $N > 240$ data points were least-square fit to Eq. 2, resulting in a parameter set $\{r_1^2(t_{lag}), r_2^2(t_{lag}), \alpha\}$ for each time lag, t_{lag}, between 5 and 60 ms. This approach of fitting leads to a robust estimation of the mean-square displacements r_1^2 and r_2^2 even when the mobility is not purely random (23).

Mobility analysis

By plotting r_1^2 and r_2^2 versus t_{lag}, the diffusional behavior of the respective populations of molecules is revealed. The (r_i^2,t_{lag}) plots were fitted either by a free diffusion model ($r_i^2 = 4D_i t_{lag}$) or by a confined diffusion model. The confined diffusion model assumes that diffusion is free within a square of side length L, surrounded by an impermeable, reflecting barrier. In such a model the mean-square displacement depends on L and the instantaneous diffusion constant D_o, and varies with t_{lag} as (28):

$$r_i^2(t_{lag}) = \frac{L^2}{3} \times \left(1 - \exp\left(\frac{-12D_0 t_{lag}}{L^2}\right)\right). \quad (3)$$

For the analysis of the (r_i^2,t_{lag}) plots, it has to be taken into account that the positional accuracy in our measurements is 35 nm, which leads to a constant offset in r_i^2 of $4 \times (35\ nm)^2 = 4.9 \times 10^3\ nm^2$ for all time lags (24). From this positional accuracy, we estimate that domains of size $L = \sqrt{(3 \times 4.9 \times 10^3 nm^2)} = 121nm$ represent the smallest domains that could be observed. This domain size corresponds to a diameter of ~137 nm.

RESULTS

Localization of the membrane anchors and observation of single-molecules

The LckN11-eYFP construct was obtained by fusing the membrane anchoring sequence (11 N-terminal amino-acids)

of the Src kinase Lck to the N-terminus of eYFP. When expressed in mammalian cells this fusion protein is anchored to the cytoplasmic leaflet of the plasma membrane via two cysteine-linked S-acyl groups and one glycine-linked myristoyl group (Fig. 1 *A*). Transient transfection of 3T3-A14 cells with the LckN11-eYFP construct resulted in a clear plasma membrane localization of fluorescence (Fig. 1 *B*). The eYFP-C14KRas construct consists of the 14 C-terminal amino-acids of K-Ras fused to the C-terminus of eYFP (Fig. 1 *C*). Expression of this construct in 3T3-A14 cells revealed membrane localization of the fluorescence (Fig. 1 *D*). To obtain a low density of membrane-anchored eYFP molecules at the plasma membrane ($<1\ \mu m^{-2}$), 3T3-A14 cells were used for single-molecule microscopy 5–6 days after transfection.

For the diffusion measurements the focus was set to the apical membrane, where single-molecule signals were observed (Fig. 2 *A*). These signals displayed single-step photobleaching behavior (Fig. 2 *B*), which is indicative for the observation of individual fluorophores. The observation of single eYFP molecules is further confirmed by analysis of the measured signal intensities. The intensity distributions (Fig. 2 *C*) closely resemble that of monomeric eYFP observed before (23,29) and peak at 208 counts/3 ms for LckN11-eYFP and 200 counts/3 ms for eYFP-C14KRas. A comparison of these signals to the background noise results in a signal/background noise ratio of ~12. Tracking of the single-molecule signals through consecutive images yielded trajectories of diffusing molecules (Fig. 2 *D*). Large numbers (>2500 per condition) of these trajectories were obtained for both the Lck and the K-Ras anchor.

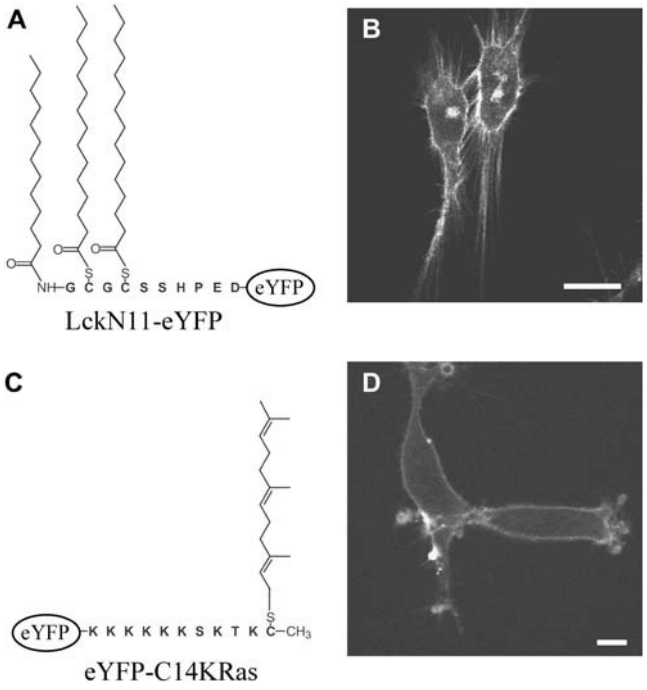

FIGURE 1 Schematic drawing of the LckN11-eYFP (*A*) and eYFP-C14KRas (*C*) constructs. The amino acids of the membrane anchoring sequences are given in bold one-letter code. Confocal fluorescence images of 3T3-A14 cells expressing LckN11-eYFP (*B*) and 3T3-A14 cells expressing eYFP-C14KRas (*D*) 2 days after transfection. Clear plasma membrane localization was observed for both constructs. Scale bar, 10 μm.

Cumulative probability distributions of the square displacement

The trajectories of diffusing LckN11-eYFP and eYFP-C14KRas molecules were used to construct square displacement distributions. From these, the cumulative probability distribution was built and plotted versus the square displacement, as shown in Fig. 3, *A* and *B*, for a time lag of 40 ms and 60 ms, respectively. The distribution of the K-Ras anchor was clearly shifted to lower r^2 values compared to that of the Lck membrane anchor, an indication that the K-Ras anchor had a lower overall mobility. The distributions of both the Lck membrane anchor and the K-Ras membrane anchor could not be fitted by a one-component model (*dashed line*, Fig. 3, *C* and *D*; Eq. 1, Materials and Methods), which assumed one population of diffusing particles. The fit improved significantly (*solid line*, Fig. 3, *C* and *D*) by the use of a two-component model (Eq. 2, Materials and Methods), which assumed two populations of diffusing molecules to be present. Extension of the model with an additional population, resulting in a three-component model, did not improve the fit significantly. Hence, the two-component model was used to fit the cumulative probability distributions of the square displacement.

A fit of a cumulative probability distribution of the square displacement to this two-component model resulted in a parameter set consisting of: the fraction, α, of fast diffusing molecules and the characteristic mean-square displacements, r_1^2 and r_2^2, for the fast- and slow-diffusing fraction of molecules, respectively. For LckN11-eYFP (Fig. 3 *C*) a fit of 40 ms time-lag data according to Eq. 2 resulted in values of 0.84 ± 0.04, 0.20 ± 0.02 μm^2, and 0.015 ± 0.008 μm^2 for α, r_1^2, and r_2^2, respectively. For eYFP-C14KRas (Fig. 3 *D*) a fit according to Eq. 2 yielded 0.62 ± 0.13, 0.16 ± 0.04 μm^2, and 0.021 ± 0.009 μm^2 for α, r_1^2, and r_2^2, respectively. The fraction of fast-diffusing molecules, α, was significantly larger for the Lck membrane anchor compared to that of the K-Ras membrane anchor, in agreement with the difference in the square displacement distributions of Fig. 3, *A* and *B*.

Diffusion analysis of the Lck and K-Ras membrane anchor

Cumulative probability distributions like the ones presented in Fig. 3 were obtained for different time lags, varying from 5–60 ms. For all time lags and constructs measured, the cumulative probability distributions exhibited a biphasic behavior and were fitted to the two-component model (Eq. 2). As described, these fits result in a set of parameters for each time

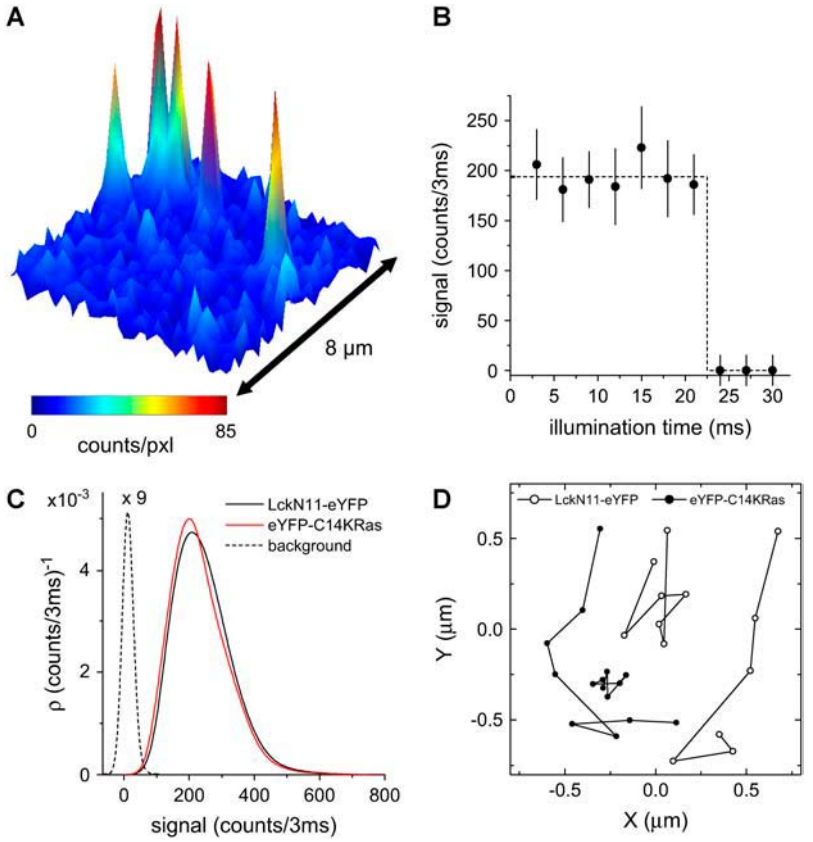

FIGURE 2 (*A*) Image showing five signals of individual LckN11-eYFP molecules at the apical membrane of a 3T3-A14 cell. (*B*) Example of a single-step photobleaching event of an LckN11-eYFP molecule. (*C*) Probability densities of the intensities of 3033 LckN11-eYFP molecules (*black solid line*) and 365 eYFP-C14KRas molecules (*red solid line*) observed at the apical membrane of 3T3-A14 cells. The distributions were nearly Gaussian-shaped with maxima of 208 counts/3 ms for LckN11-eYFP and 200 counts/3 ms for eYFP-C14KRas. The probability density of the background signal (*dashed line*) was characterized by a width of 17 counts/3 ms. (*D*) Trajectories of LckN11-eYFP molecules (*open circles*) and eYFP-C14KRas (*solid circles*) diffusing at the apical membrane of a 3T3-A14 cell. The time between consecutive points (time lag) was 20 ms. Data for all figures shown were obtained with an illumination intensity of 2 kW/cm^2 and illumination time of 3 ms.

lag. For LckN11-eYFP, these parameter sets were plotted versus time lag in Fig. 4, *A–C*. The fast-diffusing LckN11-eYFP molecules represented the largest fraction of molecules (Fig. 4 *A*). This fraction was constant between 5 and 60 ms with a weighted mean of 0.84 ± 0.03 (mean ± SE; *solid line*). The mean-square displacement of the fast fraction, r_1^2, exhibited a linear increase with time predicted for a free-diffusing species. A fit of these data to a free-diffusion model, $r_1^2 = 4D_1t$ (Fig. 4 *B*, *solid line*), resulted in a diffusion coefficient of $D_1 = 1.30 \pm 0.03$ μm^2/s. The remaining fraction, containing ~16% of the LckN11-eYFP molecules, displayed a lower mobility (Fig. 4 *C*). Moreover, the mean-square displacement leveled off to a constant value of $2.1 \pm 0.8 \times 10^{-2}$ μm^2 for longer time lags, an indication of confined diffusion. A fit of the data to a confined diffusion model (Eq. 3), resulted in an instantaneous diffusion coefficient, D_0, of 0.26 ± 0.13 μm^2/s and an average domain size of $L = 221 \pm 49$ nm (Table 1).

The results of the diffusion analysis of the K-Ras membrane anchor are shown in Fig. 4, *D* and *E*. As found for the Lck membrane anchor, the fast-diffusing fraction of the K-Ras membrane anchor is constant between 5 and 60 ms and contained the majority of molecules. The weighted mean of 0.73 ± 0.04 is slightly smaller than the weighted mean of the Lck membrane anchor. Analogous to the Lck membrane anchor, the mean-square displacement of the fast fraction of eYFP-C14KRas showed a linear increase with time (Fig. 4 *E*), predicted for free-diffusing particles. A fit of these data to a free-diffusion model yielded a diffusion coefficient of $D_1 = 1.00 \pm 0.04$ μm^2/s, ~23% smaller than the value found for the Lck membrane anchor. The remaining, slow-diffusing fraction contained 27% of the eYFP-C14KRas molecules and displayed a lower mobility (Fig. 4 *F*). As observed for the Lck membrane anchor, the mean-square displacement of the slow-diffusing fraction of the K-Ras membrane anchor leveled-off at longer time lags (Fig. 4 *F*), indicating confined diffusion. A fit of the data to a confined diffusion model (Eq. 3), resulted in an instantaneous diffusion coefficient, $D_0 = 0.15 \pm 0.05$ μm^2/s and an average domain size of $L = 219 \pm 71$ nm (Table 1).

DISCUSSION

As outlined in the introduction, the aim of this study was to compare the diffusion behavior of the K-Ras anchor, which supposedly has negligible affinity toward lipid rafts and the Lck membrane anchor, which has been assigned a high affinity for lipid rafts. Using single-molecule fluorescence microscopy we were able to study the diffusion of these anchors with high spatial (~35 nm) and temporal (~10 ms) accuracy. This accuracy allowed the detection of membrane domains with a diameter larger than ~137 nm (see Materials and Methods).

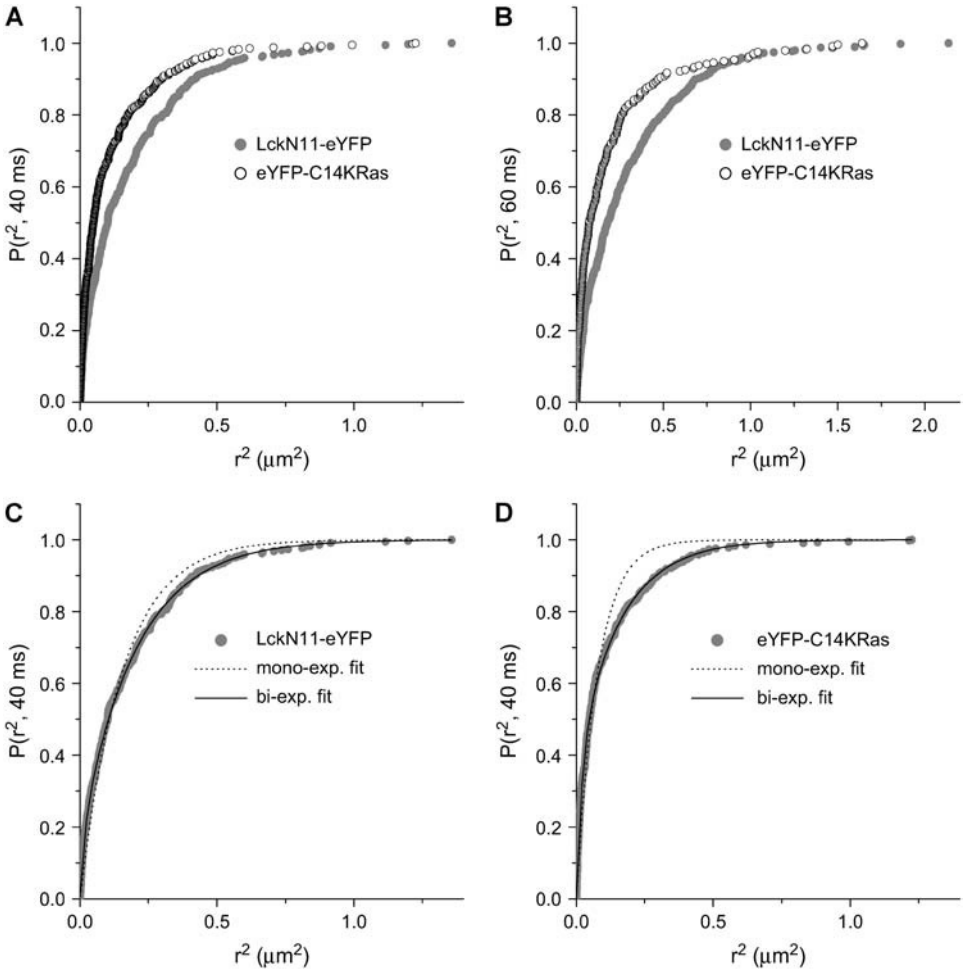

FIGURE 3 Cumulative probability, $P(r^2,t_{lag})$, versus the square displacements, r^2 for LckN11-eYFP (*shaded circles* and eYFP-C14KRas (*open circles*) with a time lag of 40 ms (*A*) and 60 ms (*B*). Each data set contained at least 200 data points. For both time lags, the eYFP-C14KRas data showed a clear shift to lower r^2 values compared to the LckN11-eYFP data. Fits to a one-component model (Eq. 1 Materials and Methods, *dashed line*) and a two-component model (Eq. 2, *solid line*) of the 40 ms time lag data of LckN11-eYFP (*C*) and eYFP-C14KRas (*D*).

Although we did observe differences in the diffusion behavior of the K-Ras and Lck membrane anchor, there was a clear overall similarity. Both anchors showed a major, fast-diffusing fraction (Table 1), that diffused freely on the timescale measured (~10–60 ms) with a diffusion coefficient (1–1.3 $\mu m^2/s$) that is comparable to those measured for lipids in the exoplasmic leaflet (0.6–1.6 $\mu m^2/s$) (2,10). Only a minor fraction (16% for the Lck anchor and 27% for the K-Ras anchor) of molecules had a lower mobility and was confined to domains of size ~200 nm (Table 1). The fact that the Lck membrane anchor showed predominantly free diffusion is in agreement with other single-molecule studies of this anchor (30,31), which reported diffusion coefficients of 0.5–1.0 $\mu m^2/s$ on the ~100-ms timescale.

If the diffusion characteristics of the Lck membrane anchor, the K-Ras membrane anchor and, in addition, the H-Ras membrane anchor (23) are compared, it is striking that all exhibit a major, fast-diffusing fraction and a minor, slow-diffusing fraction. For all anchors, the fast fraction diffused freely on a timescale up to ~60 ms and increased from 59 ± 7% for the H-Ras anchor to 73 ± 4% for the K-Ras anchor and 84 ± 3%, for the Lck anchor. The diffusion coefficients of the fast-diffusing fraction of the H-Ras anchor (1.13 ± 0.09 $\mu m^2/s$) and for the K-Ras anchor (1.00 ± 0.04 $\mu m^2/s$) are not significantly different, but lower by ~20% than that found for the Lck anchor (1.30 ± 0.03 $\mu m^2/s$). These results indicate that, if rafts are present, the anchors with high raft affinity (Lck and H-Ras) were not significantly slowed-down compared to the nonraft K-Ras anchor. Indeed, the diffusion of the Lck anchor seems to be the highest of all membrane anchors we studied. Although our study does not exclude the existence of cytoplasmic lipid rafts, these results indicate that their effect on the mobility would have to be relatively small as would be expected from very small domains or lipid shells (32,33). This notion is in agreement with a recent FRAP study of putative raft-associated proteins at the cells surface (34), which showed that raft proteins diffuse freely over large distances and do not undergo long-range diffusion as part of discrete, stable raft domains.

Further comparison of the Lck, K-Ras, and H-Ras anchor showed that, besides the major fast-diffusing fraction, all anchors include a slow-diffusing fraction of molecules. The proportion of this slow-diffusing fraction was 41 ± 7%, 27 ± 4%, and 16 ± 3% for the H-Ras, K-Ras, and Lck

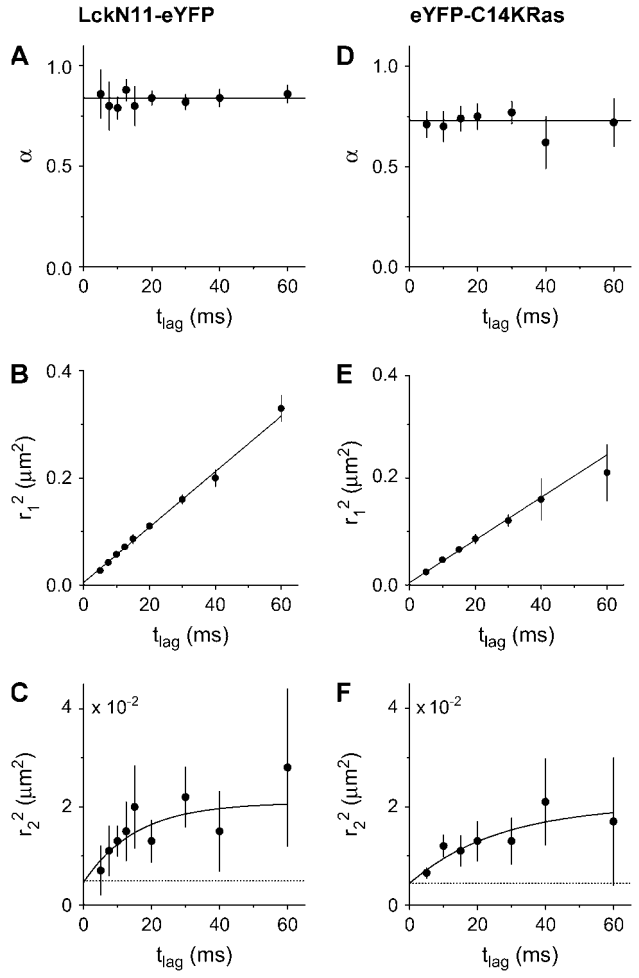

FIGURE 4 Diffusion characteristics of LckN11-eYFP (Fig. 4, *A–C*) and eYFP-C14KRas (Fig. 4, *D–F*) resulting from the square displacement distribution analysis (see Materials and Methods). (*A* and *D*) The fractions of the fast diffusing component, α, were plotted versus t_{lag}. The solid lines represent the weighted mean of the fast-diffusing fraction over all time lags. (*B* and *E*) The mean-square displacements, r_1^2, of the fast fraction plotted versus t_{lag}. The data were fitted according to a free-diffusion model ($r_1^2 = 4D_1t_{lag}$, *solid line*). (*C* and *F*) The mean-square displacements, r_2^2 of the slow fraction plotted versus t_{lag}. Fits according to a confined diffusion model (Eq. 3) are shown as a solid line. The dotted lines in Fig. 4, *C* and *F*, represent the offset due to the limited positional accuracy (see Materials and Methods); although the same offset is present in Fig. 4, *B* and *E*, the dotted lines are omitted here for clarity.

anchor respectively (Table 1). More striking is that for all anchors, this slow-diffusing fraction is confined to domains of size ~200 nm. The instantaneous diffusion constant (D_0) within these domains was identical for all anchors (Table 1) and ~0.2 $\mu m^2/s$. As the supposedly nonraft K-Ras anchor was trapped in 200-nm domains to a larger extent than the Lck anchor, it seems unlikely that the 200-nm domains seen are lipid rafts.

The association of Ras with membrane domains was recently investigated by fluorescence recovery after photobleaching (35) and electron microscopy (15,36) resulting in a model in which ~30% of the H-Ras anchor is found in cholesterol-dependent nanoclusters of ~20-nm diameter, whereas the remaining ~70% of H-Ras anchors is present as monomers. Although these nanoclusters are much smaller than the smallest domains we can detect (~137-nm diameter), it is interesting to note that the fraction of H-Ras anchor localized in the nanoclusters (~30%) corresponds reasonably well to the size of the fraction H-Ras anchor molecules localized in the 200-nm domains (27–41%, (23)), indicating that there may be a link between these observations. As it was further shown that the nanoclusters are sensitive to mild latrunculin treatment, a possible explanation for the observed 200-nm domains is temporal trapping of the 20-nm nanoclusters by the membrane-associated actin cytoskeleton and the proteins bound to it (2). The fast, free-diffusing fraction observed for the H-Ras and Lck membrane anchor would in this case be explained by the fact that the majority of the anchors move in and out of the nanoclusters on a timescale that cannot be resolved (<10 ms) by our measurements, a mechanism recently suggested in a single-molecule study of H-Ras (37). As the EM experiments further showed that the K-Ras membrane anchor is localized in separate nanoclusters, a similar mechanism could explain the observation of the 200-nm domains for the K-Ras anchor.

TABLE 1 Summary of diffusion characteristics

	LckN11-eYFP	eYFP-C14KRas	eYFP-C10HRas*
α	0.84 ± 0.03	0.73 ± 0.04	0.59 ± 0.07
D_1 ($\mu m^2/s$)	1.30 ± 0.03	1.00 ± 0.04	1.13 ± 0.09
D_0 ($\mu m^2/s$)	0.26 ± 0.13	0.15 ± 0.05	0.29 ± 0.12
L (nm)	221 ± 49	219 ± 71	206 ± 35

*Values taken from Lommerse et al. (23).

If the 200-nm domains are indeed observed because the H-Ras and Lck anchors are localized in cholesterol-dependent nanoclusters, one would expect that cholesterol depletion would affect the fraction of molecules trapped in them. We performed cholesterol depletion by methyl-β-cyclodextrin (5 mM for 1 h), but this treatment did not have a significant effect on the H-Ras anchor (23). This lack of effect can be understood in the light of recent evidence that methyl-β-cyclodextrin stabilizes the actin cytoskeleton (38). Actin stabilization would counteract the cholesterol depletion effect in our diffusion measurements and explain the observations. We tried an alternative cholesterol depletion method using compactin (see Supplementary Material), but this resulted in localization of the Lck membrane anchor to intracellular structures that made reliable single-molecule measurements on our wide-field setup impossible (see Supplemental Material, Fig. S1 and S2).

To show that the 200-nm domains are actin-dependent one might propose a mild latrunculin treatment (2), which would be expected to result in an increased size of the 200-nm domains and/or a lower fraction of molecules trapped in them. However, Fuijwara et al., showed that mild latrunculin

treatment results in a decreased hop rate and increased compartment size, which have counteracting effects on the macroscopic (>10 ms) diffusion that we measure with our technique. To separate these counteracting effects and reliably measure the net effect on the 200-nm domains a much higher time resolution is required (Fuijwara et al. used 25 μs), which cannot be achieved by a single-fluorophore technique.

In conclusion, in the current single-molecule diffusion study we compared the nonraft K-Ras anchor and the raft-associated Lck anchor and showed that there are strong similarities in diffusion behavior of these anchors. The lack of clear differences between the two membrane anchors supports models of the cytoplasmic leaflet in which potential lipid rafts are small (<137 nm diameter) and do not have a large impact on the mobility of putative raft-associated molecules on the 10–60 ms timescale.

SUPPLEMENTARY MATERIAL

An online supplement to this article can be found by visiting BJ Online at http://www.biophysj.org.

The 3T3-A14 cells were a generous gift from Dr. D. M. Ouwens and Dr. J. A. Maassen, Leiden University Medical Center. We thank A. A. de Boer for maintenance of the cell cultures and G. A. Blab for help with the data analysis. We thank Dr. J. Hancock for the gift of the K-Ras membrane anchor construct.

This work was supported by funds from Aard- en Levenswetenschappen (ALW), Stichting voor Fundamenteel Onderzoek der Materie (FOM) and Nederlandse Organisatie voor Wetenschappelijk Onderzoek (NWO) program for Physical Biology (99FBK03), the CYTTRON consortium sponsored by a grant from the Dutch Ministry of Economic Affairs for and the UK Medical Research Council (grant No. G0100471, AIM; studentship No. G78/6530, NJP).

REFERENCES

1. Vereb, G., J. Szollosi, J. Matko, P. Nagy, T. Farkas, L. Vigh, L. Matyus, T. A. Waldmann, and S. Damjanovich. 2003. Dynamic, yet structured: the cell membrane three decades after the Singer-Nicolson model. *Proc. Natl. Acad. Sci. USA.* 100:8053–8058.
2. Fujiwara, T., K. Ritchie, H. Murakoshi, K. Jacobson, and A. Kusumi. 2002. Phospholipids undergo hop diffusion in compartmentalized cell membrane. *J. Cell Biol.* 157:1071–1081.
3. van Meer, G., and K. Simons. 1988. Lipid polarity and sorting in epithelial cells. *J. Cell. Biochem.* 36:51–58.
4. Simons, K., and E. Ikonen. 1997. Functional rafts in cell membranes. *Nature.* 387:569–572.
5. Brown, D. A., and J. K. Rose. 1992. Sorting of GPI-anchored proteins to glycolipid-enriched membrane subdomains during transport to the apical cell surface. *Cell.* 68:533–544.
6. Simons, K., and D. Toomre. 2000. Lipid rafts and signal transduction. *Nat. Rev. Mol. Cell Biol.* 1:31–39.
7. Sheets, E. D., G. M. Lee, R. Simson, and K. Jacobson. 1997. Transient confinement of a glycosylphosphatidylinositol-anchored protein in the plasma membrane. *Biochemistry.* 36:12449–12458.
8. Varma, R., and S. Mayor. 1998. GPI-anchored proteins are organized in submicron domains at the cell surface. *Nature.* 394:798–801.
9. Pralle, A., P. Keller, E. L. Florin, K. Simons, and J. K. Hörber. 2000. Sphingolipid-cholesterol rafts diffuse as small entities in the plasma membrane of mammalian cells. *J. Cell Biol.* 148:997–1008.
10. Schütz, G. J., G. Kada, V. P. Pastushenko, and H. Schindler. 2000. Properties of lipid microdomains in a muscle cell membrane visualized by single molecule microscopy. *EMBO J.* 19:892–901.
11. Dietrich, C., B. Yang, T. Fujiwara, A. Kusumi, and K. Jacobson. 2002. Relationship of lipid rafts to transient confinement zones detected by single particle tracking. *Biophys. J.* 82:274–284.
12. Sharma, P., R. Varma, R. C. Sarasij, Ira, K. Gousset, G. Krishnamoorthy, M. Rao, and S. Mayor. 2004. Nanoscale organization of multiple GPI-anchored proteins in living cell membranes. *Cell.* 116:577–589.
13. Wang, T. Y., and J. R. Silvius. 2001. Cholesterol does not induce segregation of liquid-ordered domains in bilayers modeling the inner leaflet of the plasma membrane. *Biophys. J.* 81:2762–2773.
14. Zacharias, D. A., J. D. Violin, A. C. Newton, and R. Y. Tsien. 2002. Partitioning of lipid-modified monomeric GFPs into membrane microdomains of live cells. *Science.* 296:913–916.
15. Prior, I. A., C. Muncke, R. G. Parton, and J. F. Hancock. 2003. Direct visualization of Ras proteins in spatially distinct cell surface microdomains. *J. Cell Biol.* 160:165–170.
16. Rodgers, W., B. Crise, and J. K. Rose. 1994. Signals determining protein tyrosine kinase and glycosyl-phosphatidylinositol-anchored protein targeting to a glycolipid-enriched membrane fraction. *Mol. Cell. Biol.* 14:5384–5391.
17. Shenoy-Scaria, A. M., D. J. Dietzen, J. Kwong, D. C. Link, and D. M. Lublin. 1994. Cysteine3 of Src family protein tyrosine kinase determines palmitoylation and localization in caveolae. *J. Cell Biol.* 126: 353–363.
18. Janes, P. W., S. C. Ley, and A. I. Magee. 1999. Aggregation of lipid rafts accompanies signaling via the T cell antigen receptor. *J. Cell Biol.* 147:447–461.
19. Kabouridis, P. S., A. I. Magee, and S. C. Ley. 1997. S-acylation of LCK protein tyrosine kinase is essential for its signalling function in T lymphocytes. *EMBO J.* 16:4983–4998.
20. Apolloni, A., I. A. Prior, M. Lindsay, R. G. Parton, and J. F. Hancock. 2000. H-ras but not K-Ras traffics to the plasma membrane through the exocytic pathway. *Mol. Cell. Biol.* 20:2475–2487.
21. Schmidt, T., G. J. Schütz, W. Baumgartner, H. J. Gruber, and H. Schindler. 1995. Characterization of photophysics and mobility of single molecules in a fluid lipid membrane. *J. Phys. Chem.* 99:17662–17668.
22. Harms, G. S., L. Cognet, P. H. Lommerse, G. A. Blab, and T. Schmidt. 2001. Autofluorescent proteins in single-molecule research: applications to live cell imaging microscopy. *Biophys. J.* 80:2396–2408.
23. Lommerse, P. H. M., G. A. Blab, L. Cognet, G. S. Harms, B. E. Snaar-Jagalska, H. P. Spaink, and T. Schmidt. 2004. Single-molecule imaging of the H-Ras membrane-anchor reveals domains in the cytoplasmic leaflet of the cell membrane. *Biophys. J.* 86:609–616.
24. Schütz, G. J., H. Schindler, and T. Schmidt. 1997. Single-molecule microscopy on model membranes reveals anomalous diffusion. *Biophys. J.* 73:1073–1080.
25. Anderson, C. M., G. N. Georgiou, I. E. Morrison, G. V. Stevenson, and R. J. Cherry. 1992. Tracking of cell surface receptors by fluorescence digital imaging microscopy using a charge-coupled device camera. Low-density lipoprotein and influenza virus receptor mobility at 4 degrees C. *J. Cell Sci.* 101:415–425.
26. Almeida, P. F. F., and W. L. C. Vaz. 1995. Lateral diffusion in membranes. R. Lipowsky, and E. Sackmann, editors. Elsevier/North Holland, Amsterdam. 305–357.
27. Sonnleitner, A., G. J. Schütz, and T. Schmidt. 1999. Free Brownian motion of individual lipid molecules in biomembranes. *Biophys. J.* 77:2638–2642.
28. Kusumi, A., Y. Sako, and M. Yamamoto. 1993. Confined lateral diffusion of membrane receptors as studied by single particle tracking (nanovid microscopy). Effects of calcium-induced differentiation in cultured epithelial cells. *Biophys. J.* 65:2021–2040.

29. Lommerse, P. H. M., B. E. Snaar-Jagalska, H. P. Spaink, and T. Schmidt. 2005. Single-molecule diffusion measurements of H-Ras at the plasma membrane of live cells reveal microdomain localization upon activation. *J. Cell Sci.* 118:1799–1809.

30. Ike, H., A. Kosugi, A. Kato, R. Iino, H. Hirano, T. Fujiwara, K. Ritchie, and A. Kusumi. 2003. Mechanism of Lck recruitment to the T-cell receptor cluster as studied by single-molecule-fluorescence video imaging. *ChemPhysChem.* 4:620–626.

31. Douglass, A. D., and R. D. Vale. 2005. Single-molecule microscopy reveals plasma membrane microdomains created by protein-protein networks that exclude or trap signaling molecules in T cells. *Cell.* 121:937–950.

32. Saffman, P. G., and M. Delbrück. 1975. Brownian motion in biological membranes. *Proc. Natl. Acad. Sci. USA.* 72:3111–3113.

33. Anderson, R. G., and K. Jacobson. 2002. A role for lipid shells in targeting proteins to caveolae, rafts, and other lipid domains. *Science.* 296:1821–1825.

34. Kenworthy, A. K., B. J. Nichols, C. L. Remmert, G. M. Hendrix, M. Kumar, J. Zimmerberg, and J. Lippincott-Schwartz. 2004. Dynamics of putative raft-associated proteins at the cell surface. *J. Cell Biol.* 165:735–746.

35. Niv, H., O. Gutman, Y. Kloog, and Y. I. Henis. 2002. Activated K-Ras and H-Ras display different interactions with saturable nonraft sites at the surface of live cells. *J. Cell Biol.* 157:865–872.

36. Plowman, S. J., C. Muncke, R. G. Parton, and J. F. Hancock. 2005. H-Ras, K-Ras, and inner plasma membrane raft proteins operate in nanoclusters with differential dependence on the actin cytoskeleton. *Proc. Natl. Acad. Sci. USA.* 102:15500–15505.

37. Murakoshi, H., R. Iino, T. Kobayashi, T. Fujiwara, C. Ohshima, A. Yoshimura, and A. Kusumi. 2004. Single-molecule imaging analysis of Ras activation in living cells. *Proc. Natl. Acad. Sci. USA.* 101:7317–7322.

38. Kwik, J., S. Boyle, D. Fooksman, L. Margolis, M. P. Sheetz, and M. Edidin. 2003. Membrane cholesterol, lateral mobility, and the phosphatidylinositol 4,5-bisphosphate-dependent organization of cell actin. *Proc. Natl. Acad. Sci. USA.* 100:13964–13969.